Ultimate Turbulent Taylor-Couette Flow

Sander G. Huisman,[1] Dennis P. M. van Gils,[1] Siegfried Grossmann,[2] Chao Sun,[1] and Detlef Lohse[1]

[1]*Department of Applied Physics and J. M. Burgers Centre for Fluid Dynamics, University of Twente, P.O. Box 217, 7500 AE Enschede, The Netherlands*

[2]*Department of Physics, Renthof 6, University of Marburg, D-35032 Marburg, Germany*

(Received 23 July 2011; published 9 January 2012)

The flow structure of strongly turbulent Taylor-Couette flow with Reynolds numbers up to $\mathrm{Re}_i = 2 \times 10^6$ of the inner cylinder is experimentally examined with high-speed particle image velocimetry (PIV). The wind Reynolds numbers Re_w of the turbulent Taylor-vortex flow is found to scale as $\mathrm{Re}_w \propto \mathrm{Ta}^{1/2}$, exactly as predicted by Grossmann and Lohse [Phys. Fluids **23**, 045108 (2011).] for the ultimate turbulence regime, in which the boundary layers are turbulent. The dimensionless angular velocity flux has an effective scaling of $\mathrm{Nu}_\omega \propto \mathrm{Ta}^{0.38}$, also in correspondence with turbulence in the ultimate regime. The scaling of Nu_ω is confirmed by *local* angular velocity flux measurements extracted from high-speed PIV measurements: though the flux shows huge fluctuations, its spatial and temporal average nicely agrees with the result from the global torque measurements.

DOI: 10.1103/PhysRevLett.108.024501 PACS numbers: 47.27.−i

The Taylor-Couette (TC) system is one of the fundamental geometries conceived in order to test theories in fluid dynamics. Fluid is confined between two coaxial, differentially rotating cylinders. The system has been used to measure viscosity, study hydrodynamic instabilities, pattern formation, and the flow was found to have a very rich phase diagram [1]. In the fully turbulent regime, the focus up to now has been on *global* transport quantities [2–6], which can be connected to the torque τ, which is necessary to keep the inner cylinder rotating at constant angular velocity. In Ref. [7] the analogy between the angular velocity flux in TC turbulence and the heat-flux in Rayleigh-Bénard (RB; see Ref. [8]) flow was worked out, suggesting to express the former in terms of the Nusselt number Nu_ω which in Ref. [5] was found to have an effective scaling $\mathrm{Nu}_\omega \propto \mathrm{Ta}^{0.38}$ with the Taylor number (the analog to the Rayleigh number Ra in RB flow). Such effective scaling $\mathrm{Nu} \propto \mathrm{Ra}^{0.38}$ characterizes the so-called ultimate scaling regime in RB flow [9–11]. Following these papers, Grossmann and Lohse [12] have interpreted this scaling as signature of turbulent boundary layers. They derived $\mathrm{Nu} \propto \mathrm{Ra}^{1/2} \times$ log corrections (RB) and $\mathrm{Nu}_\omega \propto \mathrm{Ta}^{1/2} \times$ log corrections (TC). The log corrections imply the effective scaling law exponent of 0.38. They also made a prediction for the accompanying scaling of the wind Reynolds number Re_w, namely

$$\mathrm{Re}_w \propto \mathrm{Ra}^{1/2} \quad \text{and} \quad \mathrm{Re}_w \propto \mathrm{Ta}^{1/2} \tag{1}$$

for RB and TC turbulence, respectively. Here the logarithmic corrections remarkably cancel out, in contrast to what Kraichnan had predicted [13] earlier, namely

$$\mathrm{Re}_w \propto \mathrm{Ra}^{1/2}(\log \mathrm{Ra})^{-1/2} \quad \text{or} \quad \mathrm{Re}_w \propto \mathrm{Ta}^{1/2}(\log \mathrm{Ta})^{-1/2}, \tag{2}$$

which leads to an effective scaling exponent of about 0.47 in the relevant turbulent regime. In order to verify the interpretation of Ref. [12] and to check the prediction (1), *local* flow measurements are required to extract the wind Reynolds number Re_w. However, what happens locally, inside the TC flow, has up to now only been studied for relatively low Reynolds numbers $\mathrm{Re} < 10^5$, and has been restricted to flow profiles and single-point statistics [2,4,14–23].

In this Letter we supply local flow measurements from high-speed particle image velocimetry (PIV) at strongly turbulent TC flow. From these we will verify that indeed $\mathrm{Re}_w \propto \mathrm{Ta}^{1/2}$. In addition, from the PIV measurements we are able to also extract *local* angular velocity fluxes. These are found to strongly fluctuate in time, but when averaged azimuthally, radially, and in time, for the lower Ta show a slight axial dependence, which we interpret as reminiscence of the turbulent Taylor vortices, and which nearly vanishes for the largest Ta we achieve.

The apparatus used for the experiments has an inner cylinder with a radius of $r_i = 0.200$ m, a transparent outer cylinder with an inner-radius of $r_o = 0.279$ m, resulting in a gap width of $d = r_o - r_i = 0.079$ m and a radius ratio $\eta = r_i/r_o = 0.716$. The height is $L = 0.927$ m implying an aspect ratio of $\Gamma = L/(r_o - r_i) = 11.7$. More details regarding the experimental facility can be found in Ref. [24]. Here we focus on the case of inner cylinder rotation and fixed outer cylinder. The local velocity is measured using PIV. We utilize the viewing ports in the top plate of the apparatus to look at the flow from the top. The flow is illuminated from the side using a pulsed Nd-YLF laser [25], creating a horizontal laser sheet. The working fluid (water) is seeded with 20 μm polyamide seeding particles, and is recorded using a high-speed camera [26]. The PIV system is operated in double-frame mode

which allows us to have a Δt far smaller than $1/f$, where f is the frame rate. The PIV measurements give us direct access to both the angular velocity $\omega(\theta, r, z, t) = u_\theta(\theta, r, z, t)/r$ and the radial velocity $u_r(\theta, r, z, t)$, simultaneously.

From the latter we extract the wind Reynolds number as $\mathrm{Re}_w := u_r^{\mathrm{std}} d/\nu$, where u_r^{std} is the standard deviation of the radial velocity. In Fig. 1 Re_w is shown as a function of the Taylor number

$$\mathrm{Ta} = \tfrac{1}{4}\sigma(r_o - r_i)^2(r_i + r_o)^2(\omega_i - \omega_o)^2/\nu^2. \quad (3)$$

In Refs. [5,7] Ta had been suggested as most appropriate independent variable of the TC system in order to work out the analogy with RB. Here $\sigma = ((1+\eta)/(2\sqrt{\eta}))^4$ can be interpreted as geometric "Prandtl number" [7], $\omega_{i,o}$ is the angular velocity of the inner and outer cylinder, respectively, and ν is the kinematic viscosity. Note that $\mathrm{Ta} \propto (\omega_i - \omega_o)^2$: while Ra in RB convection is proportional to the temperature difference times the given gravity force, Ta in TC flow is proportional to the angular velocity difference $\omega_i - \omega_o$ times the centrifugal force, which itself is also proportional to $\omega_i - \omega_o$, implying the square-dependence. Therefore, by definition, the two control parameters Re_i (referring to the imposed azimuthal velocity) and Ta are connected by $\mathrm{Re}_i \sim \mathrm{Ta}^{1/2}$, but such a trivial relation of course does not exist between the wind Reynolds number Re_w and Ta (which is a response of the systems and refers to the radial velocity).

Figure 1 reveals a clear scaling of the wind Reynolds number with the Taylor number, namely $\mathrm{Re}_w \propto \mathrm{Ta}^{0.495\pm0.010}$, which is consistent with the prediction [12]

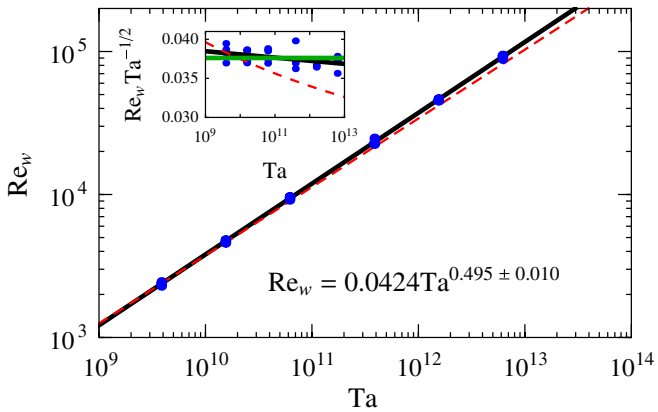

FIG. 1 (color online). Re_w vs Ta. The data from repeated experiments at midheight are plotted as separate (blue) dots, showing the quality of the reproducibility and the statistical stationarity of the measurements. We have averaged azimuthally, over time, and in the bulk flow ($0.23\ \mathrm{m} \le r \le 0.25\ \mathrm{m}$). The straight line is the best fit $\mathrm{Re}_w = 0.0424\mathrm{Ta}^{0.495\pm0.010}$ and the (red) dashed line is the Kraichnan prediction [13] Eq. (2). The inset shows the compensated plot $\mathrm{Re}_w/\mathrm{Ta}^{1/2}$ vs Ta. The horizontal (green) line is the prediction (1) of Ref. [12].

$\mathrm{Re}_w \propto \mathrm{Ta}^{1/2}$ for the ultimate TC regime, but inconsistent with Kraichnan's earlier prediction (2) of a scaling exponent $1/2$ *with* logarithmic corrections [13]. For comparison, we included this relation into Fig. 1, which clearly is inconsistent with the experimental data. We stress that the cancellation of the log-correction for Re_w as suggested in [12] is highly nontrivial and that in RB flow in the nonultimate regimes the wind Reynolds number scales as $\mathrm{Re}_w \sim \mathrm{Ra}^{0.44}$ [27], pronouncedly different than the $1/2$ exponent we find here in the ultimate regime. Only very recently the wind Reynolds number scaling in ultimate RB flow could be measured, also finding $\mathrm{Re}_w \sim \mathrm{Ra}^{1/2}$ [28] as predicted in Ref. [12].

Next, as the PIV measurements give us both the angular velocity $\omega(\theta, r, z, t)$ and the radial velocity $u_r(\theta, r, z, t)$, we can directly calculate the (total) angular velocity flux (convective + molecular)

$$J^\omega(\theta, r, z, t) := r^3(u_r\omega - \nu\partial_r\omega), \quad (4)$$

which is made dimensionless with its value for the laminar infinite aspect ratio case, $J^\omega_{\mathrm{lam}} = 2\nu r_i^2 r_o^2(\omega_i - \omega_o)/(r_o^2 - r_i^2)$, giving [7] the local "Nusselt number"

$$\mathrm{Nu}_\omega(\theta, r, z, t) = J^\omega(\theta, r, z, t)/J^\omega_{\mathrm{lam}}. \quad (5)$$

Indeed, as shown in Ref. [7], the angular velocity is the relevant quantity transported from the inner to the outer cylinder, as its flux (4) is radially conserved, once it is averaged azimuthally, axially, and over time, $\frac{d}{dr}\langle J^\omega(\theta, r, z, t)\rangle_{\theta,z,t} = 0$. In the turbulent regime the convective term is the major contributor to the flux in the bulk [29].

In Fig. 2(a) we show a snapshot of $\mathrm{Nu}(\theta, r)$ at midheight $z = L/2$ for $\mathrm{Ta} = 1.5 \times 10^{12}$. The quantity shows *huge* fluctuations, ranging from $+10^5$ to -10^5 and beyond, whereas the average $\langle \mathrm{Nu}_\omega(\theta, r, t)\rangle_{\theta,r,t} = 325$ is very close to the value $\mathrm{Nu}^{\mathrm{glob}}_\omega = 326 \pm 6$ obtained from global torque measurements [5]. The local flux can thus be more than ± 300 times as large as the mean flux. Large fluctuations have also been reported for the local heat-flux in RB flow [30], but in that case the largest fluctuations were only 25 times larger than the mean flux.

After azimuthal and time averages, $\langle \mathrm{Nu}_\omega(\theta, r, t)\rangle_{\theta,t}$, the fluctuations nearly vanish, see Fig. 2(b) (revealing some radial and height dependence for fixed $\mathrm{Ta} = 1.5 \times 10^{12}$, presumably reminiscent of the Taylor vortices) and Fig. 2(c), where we show the local angular velocity flux r' profiles for rotation rates from $\omega_i/(2\pi) = 0.5$ Hz to 20 Hz, corresponding to $\mathrm{Ta} = 3.8 \times 10^9$ to 6.2×10^{12}. Each profile is based on azimuthal averaging, radial binning, and averaging over 3200 frames (corresponding to 25.6 rotations for the three lowest rotation rates, and 32, 64, and 128 rotations for the fastest rotations rates). For each rotation rate repeated experiments have been performed and the profiles are reproducible. Only in one case the turbulent Taylor vortex flow seems to be in a different

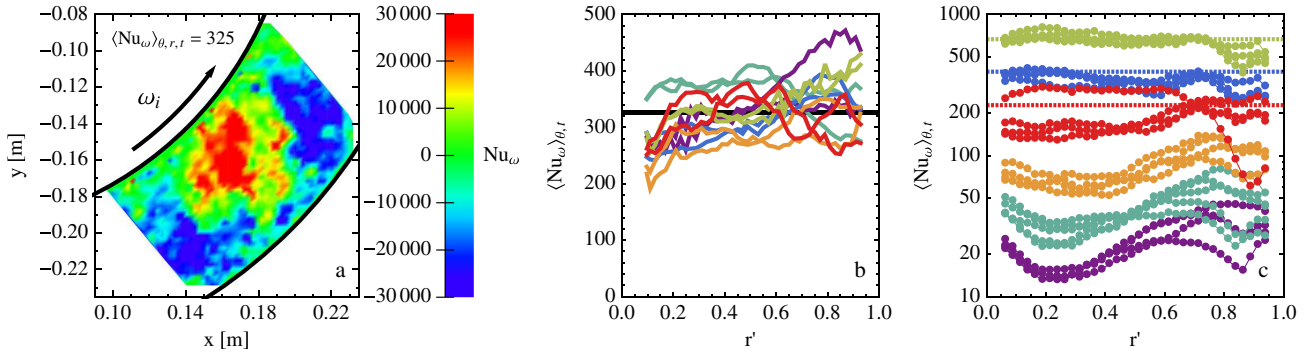

FIG. 2 (color online). (a) Snapshot of the instantaneous convective angular velocity flux, measured at $z = L/2$, for $\mathrm{Ta} = 1.5 \times 10^{12}$. The (r, θ) plane and time averaged flux is found to be equal to $\langle \mathrm{Nu}_\omega \rangle_{\theta,r,t} = 325$. A corresponding movie is available as supplemental material [33]. (b) Local normalized convective ω-flux as functions of $r' = (r - r_i)/(r_o - r_i)$ for 6 heights varying between $0.5 \leq z/L \leq 0.73$, for $\mathrm{Ta} = 1.5 \times 10^{12}$. The black solid line is the average of the 12 experiments ($\langle \mathrm{Nu}_\omega \rangle_{\theta,r,z,t}$), which is very close to the expected value 326 ± 6 from global torque measurements [5]. (c) Local normalized convective angular velocity flux vs radial position r' for various rotation rates, measured at $z = L/2$. From bottom to top we have repeated experiments for $\mathrm{Ta} = 3.8 \times 10^9$, 1.5×10^{10}, 6.2×10^{10}, 3.8×10^{11}, 1.5×10^{12}, and 6.2×10^{12}. The dashed lines for the three highest Ta represent the Nu_ω value derived from global torque measurements [5].

state(s). From Fig. 2(c) we conclude that the spread in the repeated experiments decreases with increasing Ta, for which the Taylor-vortex structure will be more and more washed out. In addition, for increasing Ta, not only do we measure during more revolutions, but also the transverse velocity increases, both improving the statistics. The dashed lines in Fig. 2(c) correspond to the measured global transport for the three highest rotation rates; these values were obtained from the torque measurements [5] and show already good agreement with our local measurements.

An additional *axial* average is necessary to obtain the exact relation between Nu_ω and the global torque τ required to drive the inner cylinder at constant velocity [7],

$$\tau = 2\pi L \rho J^{\omega}_{\mathrm{lam}} \langle \mathrm{Nu}_\omega \rangle_{\theta,z,t}. \tag{6}$$

It is the lack of sufficient axial averaging, which accounts for the small deviations between $\langle \mathrm{Nu}_\omega(\theta, z, t) \rangle_{\theta,r,t}$ and $\mathrm{Nu}_\omega^{\mathrm{glob}}$. Indeed, due to the Taylor-vortex structure of the TC flow one would expect some axial dependence of $\langle \mathrm{Nu}_\omega(\theta, r, z, t) \rangle_{\theta,r,t}$, which should become weaker with increasing degree of turbulence and thus increasing Ta, just as Fig. 2(c) suggests. This picture is confirmed in Fig. 3. Here we present local measurements of the convective angular velocity flux for varying rotation rates, resulting in a Taylor number range of 3.8×10^9–6.2×10^{12}. For each Taylor number we performed multiple experiments and measured the Nu_ω transport at midheight. The blue points are results obtained from PIV measurements at midheight, where the length of the bars indicate the error obtained from the repeated experiments. The green and orange points are repeated measurements at $z = L/2 + d/2$ and $z = L/2 + d$, respectively. An effective scaling $\mathrm{Nu}_\omega \propto \mathrm{Ta}^{0.45 \pm 0.04}$ is revealed for the blue data points, while a scaling of $\mathrm{Nu}_\omega \propto \mathrm{Ta}^{0.39 \pm 0.08}$ is revealed for the orange data points.

It is remarkable how the flow provides angular velocity transport from the inner to the outer cylinder, in spite of the fluctuative nature, which are seen in Fig. 2(a). In Fig. 4 we provide a statistical analysis of these fluctuations: While the probability distribution functions (PDFs) of the angular velocity [Fig. 4(a)] and the radial velocity [Fig. 4(b)] are nearly symmetric, the PDF of their product $r^3 u_r \omega \propto \mathrm{Nu}_\omega$ [Fig. 4(c)] is clearly positively skewed. Indeed, the

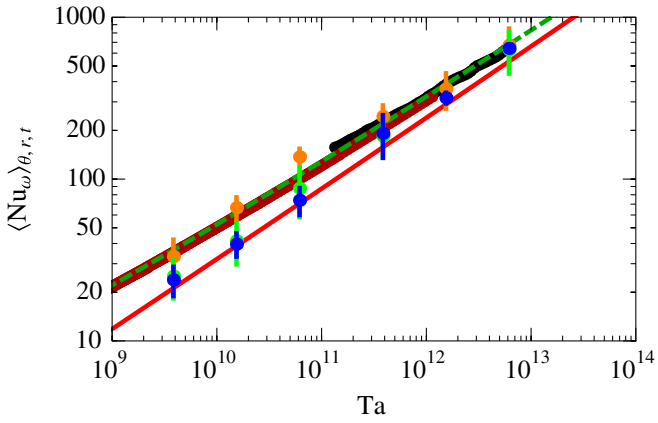

FIG. 3 (color online). Local convective angular velocity flux as a function of Taylor number. The blue dots are results obtained from PIV measurements and show a scaling of $\mathrm{Nu}_\omega \propto \mathrm{Ta}^{0.45 \pm 0.04}$. The green and orange dots are repeated measurements at a height of $z = L/2 + d/2$ and $z = L/2 + d$, respectively. The black data points are obtained from global torque measurements and show a scaling that is less steep: $\mathrm{Nu}_\omega \propto \mathrm{Ta}^{0.38}$. The dashed green line is obtained by matching two log-layers [3], and has a slope of 0.37 at $\mathrm{Ta} = 10^9$, and 0.41 at $\mathrm{Ta} = 10^{13}$. The red line is from the turbulent boundary layer theory of ref. [12]. It has a slope of 0.43 around $\mathrm{Ta} = 10^9$ and 0.44 around $\mathrm{Ta} = 10^{13}$. Dark red data points are obtained by means of global torque measurements [4].

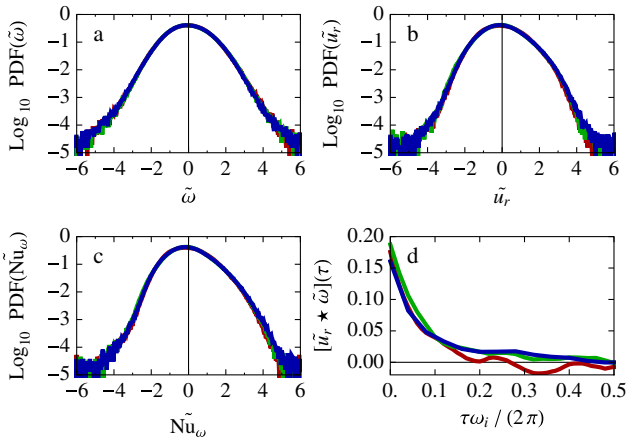

FIG. 4 (color online). Results of three experiment with varying rotation rate resulting in $\mathrm{Ta} = 3.8 \times 10^{11}$, 1.5×10^{12}, and 6.2×10^{12}, colored in red, green, and blue, respectively. All the data shown is averaged over the region $0.23\ \mathrm{m} \leq r \leq 0.25\ \mathrm{m}$, and measured at midheight. All quantities with tildes are standardized (shifted and scaled such as to have zero mean and unit variance). (a) PDF of the standardized angular velocity. (b) PDF of the standardized radial velocity. (c) Standardized normalized local convective angular velocity flux PDF. (d) Cross-correlation coefficient of the angular velocity and the radial velocity, the dimensionless decaying time (in number of rotations) is found to be 0.07. The corresponding length scale can be found by multiplying this number with the circumference of the inner cylinder giving $\delta = 88$ mm, which is of the same order of magnitude as the gap width $d = 80$ mm.

cross-correlation coefficient of u_r and ω [Fig. 4(d)] is relatively large.

We note that thanks to the PIV measurements of the full velocity field, the extraction of the local angular velocity flux $\mathrm{Nu}_\omega(\theta, r, z, t) \propto \omega u_r$ is easier in TC as compared to the analog temperature flux $\mathrm{Nu}(\vec{x}, t) \propto \mathrm{Tu}_z$ in RB flow: in order to obtain this latter quantity locally, one has to measure the temperature T and the velocity simultaneously. Because a high-precision field measurement of the temperature is presently not possible and thus not available, the best one can do for RB flow is to measure $\mathrm{Nu}(\vec{x}, t)$ point by point [30,31] or use an instrumented tracer [32].

In conclusion, from high-speed PIV measurements we have found the wind Reynolds number in strongly turbulent TC flow to scale as $\mathrm{Re}_w \propto \mathrm{Ta}^{0.495 \pm 0.010}$, in accordance with the theory of Ref. [12] and in conflict with Kraichnan's [13] prediction (2). In addition, we extracted the local angular velocity flux and found that $\mathrm{Nu}_\omega \propto \mathrm{Ta}^\gamma$ with $\gamma \sim 0.39 - 0.45$ depending on the axial position and consistent with earlier global torque measurements [5,6]. For increasing Ta, a small axial dependence of Nu_ω is fading away, reflecting the decreasing importance of the Taylor vortices. The next step will be to provide full velocity and angular velocity profile measurements, including those in the boundary layers, and to extend the present measurements to the counter-rotating case and other radii ratios η, in order to further theoretically understand the local flow organization and the interplay between bulk and boundary layers in turbulent TC flow. A further highly interesting support for the presented idea of the close correspondence between the TC angular velocity transport in the studied Ta-range with the ultimate range of RB thermal convection is to identify the onset of this ultimate range when increasing Ta; here we expect a change of the Nu_ω scaling exponent and also a transitional change in the widths and profiles of the BLs.

This study was financially supported by the Technology Foundation STW of The Netherlands.

[1] C. D. Andereck, S. S. Liu, and H. L. Swinney, J. Fluid Mech. **164**, 155 (1986).
[2] D. P. Lathrop, J. Fineberg, and H. L. Swinney, Phys. Rev. Lett. **68**, 1515 (1992).
[3] D. P. Lathrop, J. Fineberg, and H. L. Swinney, Phys. Rev. A **46**, 6390 (1992).
[4] G. S. Lewis and H. L. Swinney, Phys. Rev. E **59**, 5457 (1999).
[5] D. P. M. van Gils *et al.*, Phys. Rev. Lett. **106**, 024502 (2011).
[6] M. S. Paoletti and D. P. Lathrop, Phys. Rev. Lett. **106**, 024501 (2011).
[7] B. Eckhardt, S. Grossmann, and D. Lohse, J. Fluid Mech. **581**, 221 (2007).
[8] G. Ahlers, S. Grossmann, and D. Lohse, Rev. Mod. Phys. **81**, 503 (2009).
[9] X. Chavanne *et al.*, Phys. Rev. Lett. **79**, 3648 (1997).
[10] X. Chavanne *et al.*, Phys. Fluids **13**, 1300 (2001).
[11] G. Ahlers, D. Funfschilling, and E. Bodenschatz, New J. Phys. **13**, 049401 (2011).
[12] S. Grossmann and D. Lohse, Phys. Fluids **23**, 045108 (2011).
[13] R. H. Kraichnan, Phys. Fluids **5**, 1374 (1962).
[14] F. Wendt, Ingenieurs-Archiv **4**, 577 (1933).
[15] D. Coles and C. VanAtta, J. Fluid Mech. **25**, 513 (1996).
[16] G. Pfister and I. Rehberg, Phys. Lett. A **83**, 19 (1981).
[17] G. P. Smith and A. A. Townsend, J. Fluid Mech. **123**, 187 (1982).
[18] T. Mullin, G. Pfister, and A. Lorenzen, Phys. Fluids **25**, 1134 (1982).
[19] A. Lorenzen, G. Pfister, and T. Mullin, Phys. Fluids **96**, 236 (1983).
[20] Z.-S. She, K. Ren, G. S. Lewis, and H. L. Swinney, Phys. Rev. E **64**, 016308 (2001).
[21] J. Langenberg, M. Heise, G. Pfister, and J. Abshagen, Theor. Comput. Fluid Dyn. **18**, 97 (2004).
[22] J. Abshagen, M. Heise, C. Hoffmann, and G. Pfister, J. Fluid Mech. **607**, 199 (2008).
[23] F. Ravelet, R. Delfos, and J. Westerweel, Phys. Fluids **22**, 055103 (2010).
[24] D. P. M. van Gils *et al.*, Rev. Sci. Instrum. **82**, 025105 (2011).

[25] Litron, LDY 300 Series, dual-cavity, pulsed Nd:YLF PIV Laser System.
[26] Photron, FastCam 1024 PCI, operating at 1024 px × 1024 px resolution, and, at most, $f = 1$ kHz.
[27] X.-L. Qiu and P. Tong, Phys. Rev. E **64**, 036304 (2001).
[28] X. He *et al.*, this issue, Phys. Rev. Lett. **108**, 024502 (2012).
[29] D. P. M. van Gils *et al.* (to be published).
[30] X. D. Shang, X. L. Qiu, P. Tong, and K.-Q. Xia, Phys. Rev. Lett. **90**, 074501 (2003).
[31] X. D. Shang, P. Tong, and K.-Q. Xia, Phys. Rev. Lett. **100**, 244503 (2008).
[32] W. Shew *et al.*, Rev. Sci. Instrum. **78**, 065105 (2007).
[33] See Supplemental Material at http://link.aps.org/supplemental/10.1103/PhysRevLett.108.024501 for details and a corresponding movie.